Design of a high-speed intake distortion simulator for propulsion integration research

Matteo Migliorini[1], Artur Szymanski[2], Pavlos K Zachos[3] and David G MacManus[4]
Cranfield University, Bedfordshire, MK43 0AL, UK

Peter G Martin[5]
Defence Science and Technology Laboratory, Fareham, PO17 6AD, UK

High levels of inlet flow distortion can be a critical aspect in supersonic air induction systems due to the complex spatial nature and notable temporal unsteadiness. This can affect the operability and performance of the propulsion system. Simulation of the intake shock system in a relatively less expensive, lower technology readiness level experimental facility can be an important element to mitigate a significant part of the risk that industrial and certification testing carries. The work described in this paper is part of a programme that aims to develop such a distortion simulation test rig where the capability of advanced non-intrusive measurement techniques would be applied in propulsion integration research. The paper describes the concept, preliminary design and sizing of the working section of the rig, the exhaust system design and the integration of the test model. A brief summary of the rig architecture is provided along with details of the high-pressure system that drives the supersonic flow. The work indicates that careful design of the working section is required to ensure sufficient operating range and representative aerodynamics of the test model. It is also shown that the working section wall interference on the test model is tightly linked with the type and size of the aircraft intake to be tested. Ways to mitigate this interference are herein explored.

I. Nomenclature

A_C	Intake capture area
A_H	Working section cross-sectional area
A_0	Area of stream tube entering the inlet
A_{max}	Maximum inlet projected area,
A^*	Nozzle throat area
C_p	Static pressure coefficient
H	Working section height
H_t	Intake throat height
h	Diverter height

[1] Research Fellow, Centre for Propulsion and Thermal Power Engineering.
[2] Research Fellow, Centre for Propulsion and Thermal Power Engineering.
[3] Senior Lecturer in Propulsion Aerodynamics, Centre for Propulsion and Thermal Power Engineering, AIAA Member.
[4] Professor in Propulsion Integration, Centre for Propulsion and Thermal Power Engineering, AIAA Member.
[5] Senior Principal Scientist, Defence Science and Technology Laboratory.

l	Boundary layer plate length
M_0	Free stream Mach number at working section
n	Polytropic expansion exponent
p	Static pressure
p_f	Final pressure in vessel
p_i	Initial pressure in vessel
p_0	Stagnation pressure at settling chamber
p_∞	Free stream static pressure,
t_{run}	Rig run time
T_i	Initial temperature in vessel
T_0	Stagnation temperature at settling chamber
V	Air storage tank volume
W_{in}	Aircraft intake width

Greek letters

δ_κ	Boundary layer thickness at point of maximum profile curvature, *in*
ε	Intake flow ratio
χ	Bypass flow contraction coefficient

Abbreviations

AIP	Aerodynamic Interface Plane
PR	Pressure recovery between free stream and AIP

II. Introduction

Flow distortion in supersonic intake systems is typically of a complex spatial nature combined with notable temporal unsteadiness which may critically affect the operational stability of the propulsion system [1] [2] [3]. Future aircraft designs may feature highly three-dimensional intakes and diffusers whose design degrees of freedom will increase the complexity of integration with the propulsion system. Uncertainties in the design process could notably impact development and certification timescales. Small-scale test facilities may enable the use of advanced experimental methods to characterise unsteady distortions as well as to undertake testing of a larger number of design configurations at low cost an earlier stage in the development process. As a result, richer datasets that can used for the calibration and verification of design methods can be produced to educate and support fan design and integration with the intake system. More importantly, such test facilities could be used to de-risk and transition measurement capabilities to support larger scale fan and engine testing at higher technology readiness levels (TRL).

Previous test rigs developed for distortion simulation purposes in high-speed intakes include the configurations presented by Kimzey and Ellis [4], Surber et al [5] and Fisher and Ford [6]. Such scaled-down distortion simulators provide high-fidelity data on fan response to distortion at conditions which are representative of those in flight and build confidence in the intake-engine compatibility assessment process to be used in the earlier stages of development. In these previous cases, the shock structure around the intake entry was fully or partially generated within a relatively confined onset flow passage. These rigs were designed to provide a direct means of representing the aerodynamics of the complete air induction stream tube, albeit for a limited range of critical flight conditions, typically between nominal (critical) operation and near-nominal subcritical points with no severe instabilities of the inlet shock train. These test rigs provided a relatively simple way to explore the matching between subsonic diffusers and supersonic entries. However, the results produced were not necessarily representative of the test model's behavior during larger scale installed inlet test programmes. Reasons for these limitations include rig unstarting, interference introduced into the working sections or overall poor representativeness of the intake aerodynamics

In this paper the conceptual and preliminary design of a low TRL distortion simulation test rig is presented. The aim is to develop an experimental capability to reproduce as faithfully as possible and characterise unsteady distortions in supersonic intakes, the interactions with the diffuser flow upstream of the propulsion system and to establish methods to aid the design of future propulsion systems. For that purpose, a bespoke experimental test rig is required to enable the integration of advanced instrumentation including intrusive but more importantly non-intrusive distortion measurements at the Aerodynamic Interface Plane (AIP) of the inlet. A critical part of the test rig design is to avoid

interference of the working section walls with the inlet pre-entry flow across the widest possible mass flow range but also to ensure that the working section does not un-start, which is a typical issue with high-speed internal flow test rigs. A new motivation for such an approach is the availability of advanced experimental techniques for the measurement of internal flows, but which would currently be difficult to apply in a high-speed wind tunnel. These measurement techniques would also be difficult to apply to full-scale engine tests without previous substantial de-risking of the measurement techniques. Such techniques include non-intrusive, optical velocimetry methods such as Particle Image Velocimetry which are already demonstrated in sub-sonic configurations for dynamic distortion measurements (McLelland et al. [7], Migliorini et al. [8] and Doll et al. [9]). In addition, a scaled-down rig configuration would also enable the application of methods that can eventually offer high-resolution, rich datasets to characterise the supersonic intake entry such as dynamic pressure sensitive paint or high-speed shadowgraph techniques.

III. Intake rig overall plant architecture

An intermittent, blow down test rig configuration was selected for cost-effectiveness reasons as such supersonic test rigs are known to be less complex to develop, and have been widely adopted within university laboratory environments [5] [10] [11]. The general layout of the installation is shown in Figure 1. The system comprises an air compression plant that feeds a 50 bar 40 m^3 air receiver. When the flow arrives at approximately at a pressure of 12 bar, a double desiccant dryer with a dew point of -40°C is used to remove the water from the flow prior to it being further compressed and stored into the storage tank. Two separate sets of oil and particulate filters are located on either side of the pressure tank to improve the flow quality prior to it being introduced into the intake test rig. The pressure system supplies a settling chamber which is designed to slow down and pre-condition the flow with regards to turbulence levels and core flow uniformity (Figure 2). The design of the flow conditioners located inside the settling chamber follows the recommendations of Pope and Goin [12] and Roach [13]. The settling chamber includes provision for installation of up to three flow conditioning screens. A flow with a typical axial velocity of between 15-30 m/s is delivered from the settling chamber to the nozzle pre-contraction which in turn provides a flow with a Mach number of approximately 0.2 into the main nozzle contraction. The stagnation pressure at the settling chamber is variable and depends on the required onset Mach number at the working section. Settling chamber stagnation pressure is controlled through a segmented ball valve located at the outflow of the air storage tank (Figure 1). The segmented ball valve is connected to a quick-opening gate valves that is used to start the test rig. The throat section of the nozzle brings the flow to sonic conditions with M*=1.0, and subsequently delivers the supersonic onset flow to a square working section with dimensions of 10" x 10". The intake model is installed at a fixed angle of attack of zero, within a larger section with cross-flow area of 18"x18" (Figure 2). The mounting position of the intake with relation to the 18"x 18" working section duct is axially variable. Integration of the intake test model within the 18"x 18" working section, partially mitigates wall interference and introduces, at the same time, the notion of a semi-open jet configuration that mitigates supersonic diffuser pressure loss downstream of the working section [12]. It is also designed to allow the installation of second wall liner that could potentially be used to form the plenum chamber of a wall aspiration system should a need for such a system be realized at a later stage, for instance to enable the accurate representation of a long boundary layer diverter run-out.

A bypass system collects the excess flow, diffuses it to subsonic speeds and exhausts it radially to enable unobstructed optical access to a large part of the subsonic diffuser section of the intake (Figure 2). This allows non-intrusive optical measurements at the AIP without the potential difficulties associated with integrating optical instrumentation within the wind tunnel walls [14] [15] [16]. The radial bypass exhaust system is still under development. An intake mass flow control system is located downstream of the optical section. The mass flow control system relies on a plug nozzle that chokes a subsonic diffuser located downstream the exit of the intake duct and determines the operating condition, characterized by the Mach number at the AIP. The initial design of the plug nozzle system follows the design guidelines provided by Sasson [17] and Davis et al [18]. The mass flow control unit interface with the core exhaust system and silencers further downstream.
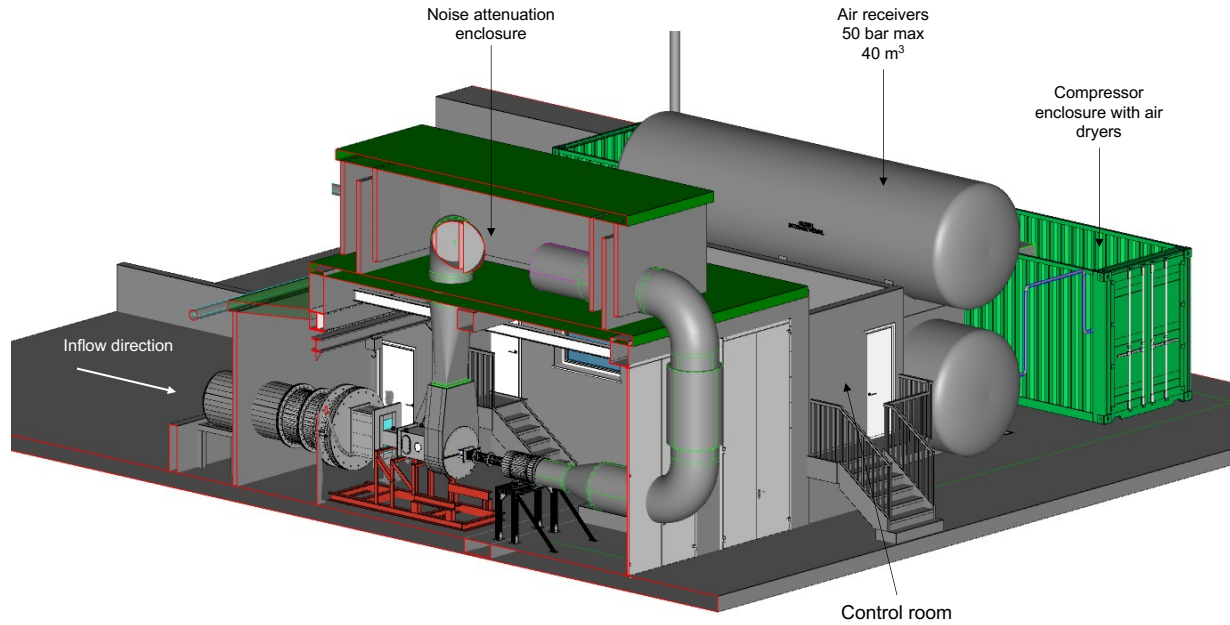
Figure 1 General layout of supersonic intake distortion test rig integrated within test cell
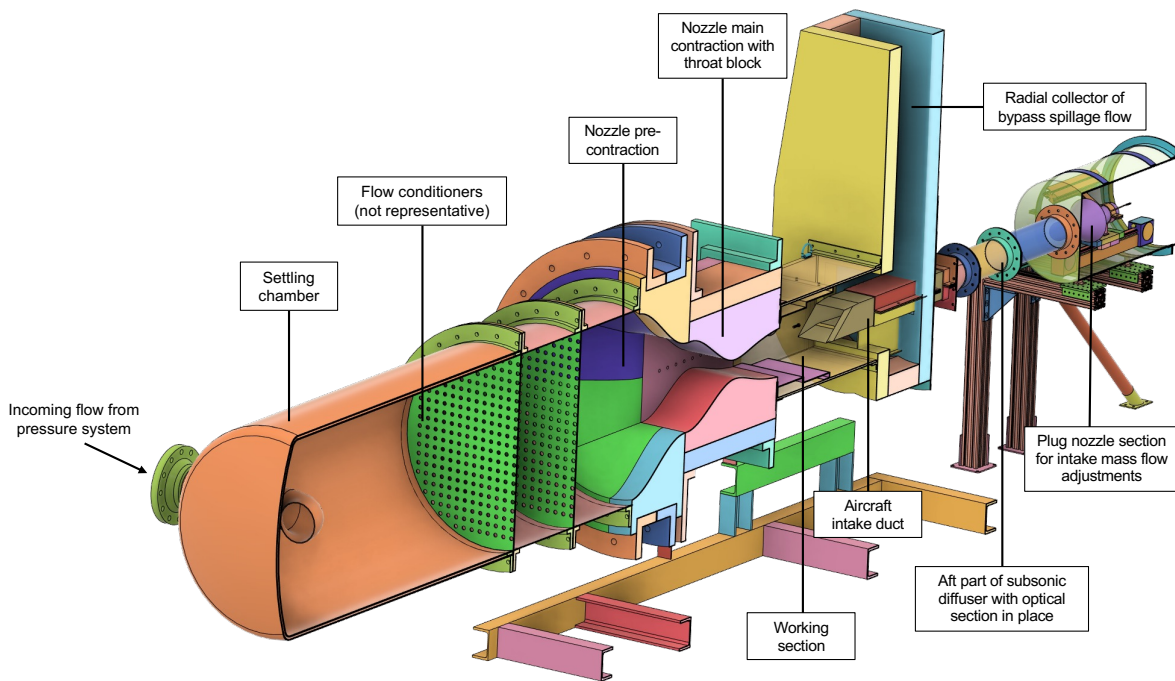

Figure 2 General arrangement of the distortion simulation rig between the settling chamber and the mass flow control section downstream of the aircraft intake duct

The intake test rig is designed to deliver a free stream Mach number, M_0, of between 1.4 to 3.0 with a baseline nominal condition of M_0=1.8. The stagnation pressure at the settling chamber (p_0) is variable and depends on the required free stream Mach at the working section. The stagnation pressure for each operating condition is highly dependent upon the pressure loss of the exhaust system and primarily upon the supersonic diffuser section which provides subsonic conditions prior to it entering the exhaust silencers. The exhaust system pressure loss, and hence the total pressure in the settling chamber, is currently estimated from CFD simulations. Based on the numerical predictions, it is estimated that p_0 will range between 2.4 bar and approximately 10.0 bar for onset Mach numbers of between 1.4 and 3.0 respectively. The stagnation temperature in the settling chamber upstream of the nozzle (T_0) is envisaged to remain almost constant during a run through provision of heat storage material in the air tank that will discharge heat to mitigate temperature drop during the transient expansion inside the air tank. This will ensure an almost constant mass flow and, more importantly, a constant Reynolds number in the working section during a single run. Based on this assumption, run time of the rig, t_{run}, was estimated using the method shown by Pope and Goin [12] for blow-down supersonic facilities operating at constant stagnation temperature, $T_i=T_0$, using the following formula:

$$t_{run} = 0.0353 \cdot \frac{V}{A^*} \cdot \frac{\sqrt{T_0}}{T_i} \cdot \frac{p_i}{p_0} \cdot \left\{ 1 - \left(\frac{p_f}{p_i} \right)^{1/n} \right\} \qquad (1)$$

In Eq. 1 , V is the air tank capacity, A^* the nozzle throat area and n the polytropic exponent that characterises the expansion of the air in the tank during operation. A value of n=1.15 was assumed during preliminary design and influenced by the intention to use high aspect ratio cylindrical air receivers to store the compressed air [12]. Subscript i indicates initial air properties at the tank whilst subscript f indicates its final condition. From Eq. 1, the estimated run time across the range of required operating conditions is shown in Figure 3a assuming a constant stagnation initial temperature of $T_i=T_0$=330 K. The estimated unit Reynolds number at the working section is shown in Figure 3b across the range of required free stream operating conditions.
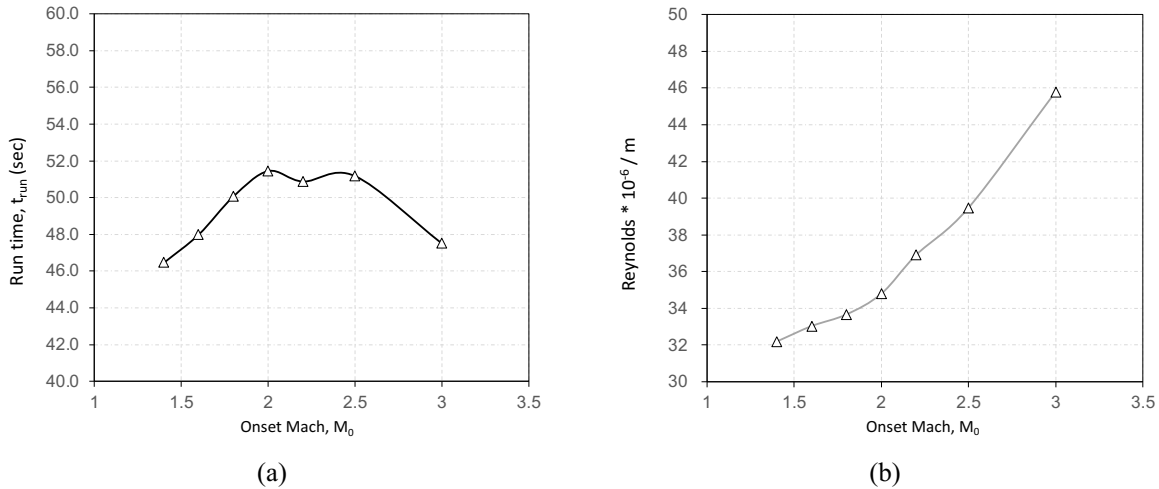

(a)   (b)

Figure 3 Estimated intake run time of the intermittent intake test rig (a) and Reynolds number per unit length (b) across the range of free stream Mach numbers for constant stagnation temperature of 330K

Based on the specified flow capacity of the compressor system, the volume of the air receiver and the desired maximum and minimum pressure during a run, it is estimated that a period between 50 minutes to an hour will be required to fully charge the air tank between consecutive runs. The estimation of the pumping time was conducted using the method shown by Pope and Goin [12].

IV. Working section design and model integration

It is known that the detailed aerodynamics near the entry of a supersonic intake can strongly influence the performance of its subsonic diffuser [14]. This is particularly important near the stability limit of the intake which influenced the need of previously developed test facilities to aid the understanding of the interactions between unsteady cowl aerodynamics and the subsonic diffuser [15] [16]. However, experimentation in sub-scale test rigs requires the integration of the intake duct within an internal flow channel where the supersonic free stream flow is delivered by a supersonic convergent-divergent nozzle system. For intermittent, blowdown facilities, the required cross-sectional area at the nozzle exit plane, hence at the inlet to the working section, is primarily influenced by the maximum achievable pressure of the inflow pressure system, the capacity of the air storage tank(s), the size of the test model and the required run time of the test rig to allow enough time for the acquisition of the required data. For a given inflow pressure system configuration, a common approach is to opt for the minimum possible nozzle cross-sectional area to enable longer testing times. When the size of the test model is known, the choice of the cross- sectional area of the working section is critical as this primarily influences the starting capability of the system [19]. Furthermore, below a certain threshold of working section area, the tunnel walls will begin to influence the flow around the test model, and can result in non-representative flow distributions which are not directly comparable with the intake operation during flight. A typical wall interference mechanism, commonly encountered in supersonic and transonic facilities, is related to shock wave reflection at the tunnel walls, which can then lead to secondary reflections on the aerodynamic surfaces of the test model [20]. The presence of such reflecting shocks alters the flow distribution around the test model which may yield misleading conclusions. The physics behind wind tunnel wall interference have been thoroughly studied in previous works, and several methods to mitigate it were proposed, such as the introduction of porous or slotted tunnel walls [12] [19]. However, the introduction of such wall treatment systems was not desired as part of the initial design of the current test rig. As a result, a simpler working section configuration was required to minimize, as much as possible, the interference on the test model without overly penalizing the desired run time which was set between 40 – 60 s.

Wall interference on the test model was quantified on a generic external compression inlet model that was developed for the purposes of the study. The geometric specification of this simple intake model corresponds to a typical external compression supersonic intake with a rectangular entry shape (Figure 4). Design shock-on-lip Mach number was 1.9. A compression ramp angle of 10° was selected such that the intake normal shock strength would be low enough to avoid shock-induced separation in the capture stream tube at the intake entry at a free stream Mach number of 1.6. The Aerodynamic Interface Plane (AIP) is located approximately at $9 \cdot \sqrt{(A_c)}$ downstream of the throat, where A_c is the geometric area at the highlight projected along the free stream direction. The nominal AIP area was equivalent to a 6" diameter and was selected based on previous experience in conducting flow distortion measurements in ducts of similar diameter with intrusive but also with optical methods. Two additional geometries with 3" and a 4.5" AIP diameter, respectively, were considered to examine the variation of wall interference as a function of the intake size for smaller scale configurations.

A preliminary analysis of the starting characteristics of a bypass section with 10"x10" constant area was conducted for a 6" AIP intake duct. Based on the definitions shown in Figure 5, the bypass flow contraction, χ, is expressed as Eq. 2 [19], as:

$$\chi = \frac{A_H - \frac{A_0}{A_c} \cdot A_c}{A_H - A_{max}} \tag{2}$$

The bypass flow contraction is a direct function of the intake's operating flow ratio, A_0/A_c expressed as the ratio between the entry area A_c and the captured stream tube area A_0. The pint of maximum cross sectional external area of the intake A_{max} forms a geometric throat in the bypass relative to the working section of area, A_H. The limiting flow contraction for starting is only a function of the free stream Mach number and gamma [19]. Hence, the contraction limit for starting of the bypass can be superimposed on the variation of the flow contraction coefficient across a typical range of intake flow ratios as shown in Figure 6. For a given AIP diameter and free stream Mach number, Figure 6 can be used to determine the minimum feasible intake flow ratio before the bypass un-starts. For example, at free stream Mach M_0=1.6, a 4.5" AIP diameter intake could operate down to 75% of capture flow ratio before the bypass section un-starts. For a 6" diameter the minimum free stream Mach number for which the bypass can potentially start is approximately M_0=1.7. However, in reality, the effective flow contraction around a practical intake could be expected to be somewhat higher than χ, and this was confirmed in later CFD analysis. A square working section of

18"x18" was finally down-selected to be integrated downstream of the 10"x10" nozzle to enable lower contraction ratios within the bypass via an enclosed open-jet configuration. As such, a transition step from 10" to the 18" cross-section would be present along all four sides of the working section. The position of this step may then be varied relative to the intake test model (L_0 in Figure 7). The 18" cross section will also provide sufficient room for a 10"x10" solid or porous wall liner to be installed in the future to enable fully installed test section operation with smaller intakes. A plenum chamber could then also be accommodated within the forward part of this section enabling wall aspiration as an optional configuration.
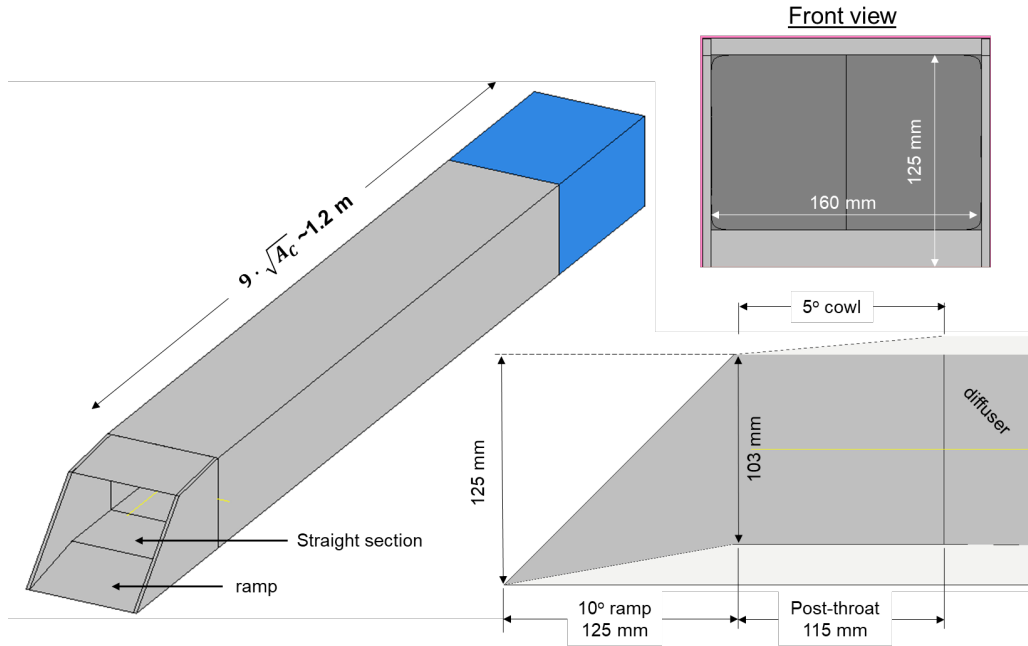
Figure 4 Generic external compression intake geometric specification
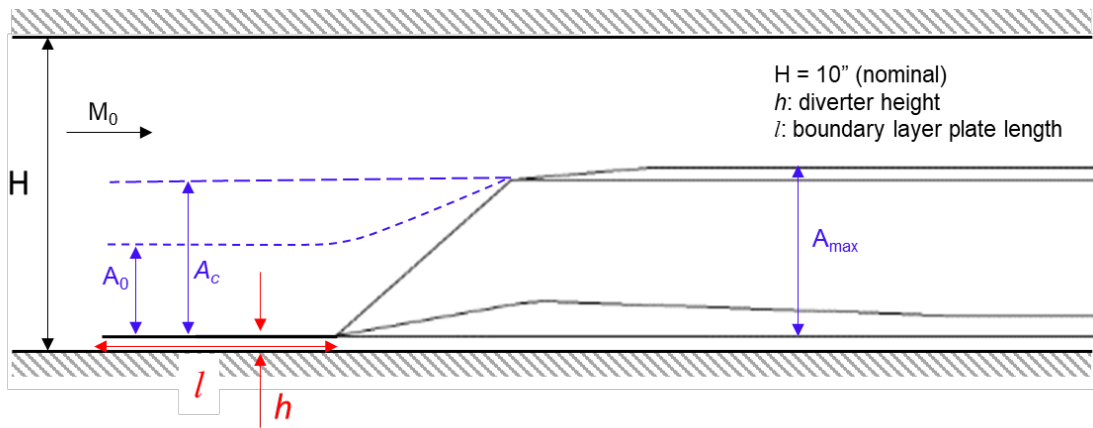
Figure 5 Schematic of generic rectangular, external compression aircraft intake integrated within a constant area, square working section of height *H*. Intake includes a diverter and a boundary player plate upstream of the compression ramp. Intake flow ratio $\varepsilon=A_0/A_c$ is directly linked to the contraction ratio of the bypass system
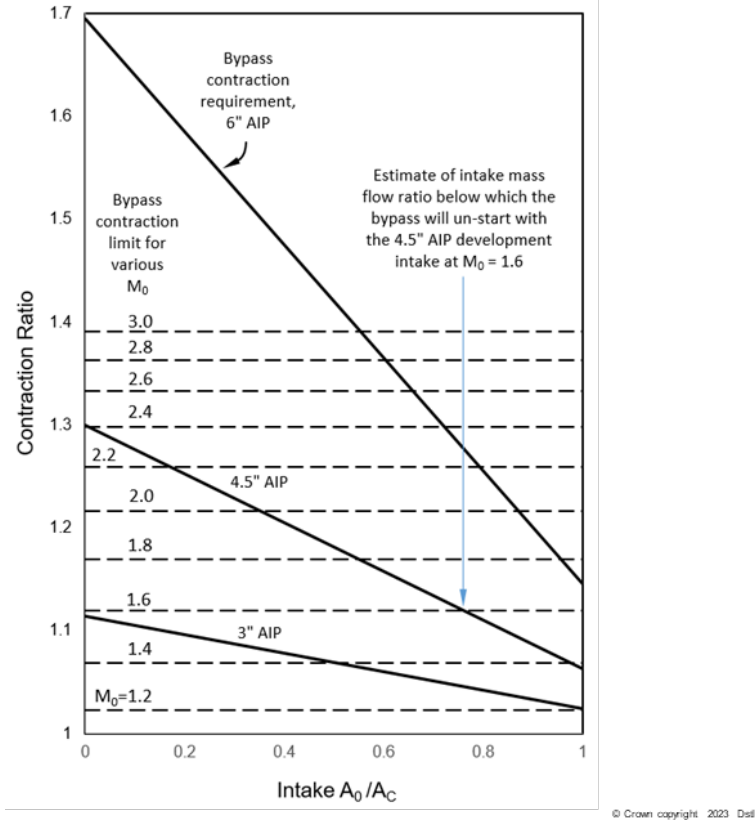
Figure 6 Ideal bypass contraction limit for starting compared to the bypass flow contraction requirement for the three development intakes across a range of mass flow ratios

To enable a systematic design process, the working section was parametrized as shown in Figure 7 where the parametric definition used for the radial exhaust diffuser is also shown. The main geometric features are a step at the top part whose position relative to the cowl lip is defined based on the H_1 and L_0 parameters. The step enables the introduction of the supersonic onset flow in the form of a semi-confined jet with the purpose of mitigating the interference of the walls on the aerodynamics of the cowl lip and enable a wider operating range of the aircraft intake. The distance between the step and the cowl lip was found to heavily influence the allowed operating range of the intake model as well as the representativeness of the lip aerodynamics with relation to the reference, isolated intake configuration. Additionally, the diverter height (*h*) and the length of a boundary layer plate (*l*) installed upstream of the intake compression ramp were also accounted for during the numerical design space explorations (Figure 5). A key design feature of the test rig is the bypass system that aims to collect entire free stream flow not ingested by the intake at each operating point (Figure 4). Unlike conventional wind-tunnel configurations, the current bypass system is also required to divert the flow radially in order to allow easier integration of instrumentation within the subsonic diffuser. Importantly, this arrangement offers optical line of sight at the intake Aerodynamic Interface Plane (AIP) which enables the use of optical methods for swirl distortion measurements at this position. It is desirable to maximise the length of the subsonic diffuser that protrudes outside of the back of the radial collector system (i.e. minimise the immersion of the supersonic entry inside the test section) without influencing the aerodynamics of the cowl or causing any un-start issues. It is also desirable to minimise the total pressure loss across the radial collector. Excessive loss in this part of the flow path would penalise the run time of the rig due to the requirement of higher settling chamber stagnation pressure, p_0, to drive the flow through the system. Finally, the radial collector should also offer an interface to the noise attenuation system through which the bypass flow is exhausted outside the test cell. As such, a radial bypass design as the one shown in Figure 7 was proposed which was previously studied in detail as part of a turbine-condenser integration system [21] [22]. The parametric definition of such radial exhaust system is also shown in Figure 7 with a 6" AIP intake installed within for reference.

Computational fluid dynamics (CFD) was used to understand the interference of the working section walls with the aerodynamics and operating range of the intake, and to develop the specification of the working section. A range of working section configurations was examined to assess their impact on the aerodynamics at the supersonic entry of the intake in relation to a reference uninstalled case, in order to establish the operating range across which the installed configuration provides sufficiently representative flow fields. The reference (uninstalled) case was defined as the same intake model in isolation. The outcome of the CFD studies was a preliminary design specification of the working section and exhaust system parameters as discussed in the following sections.
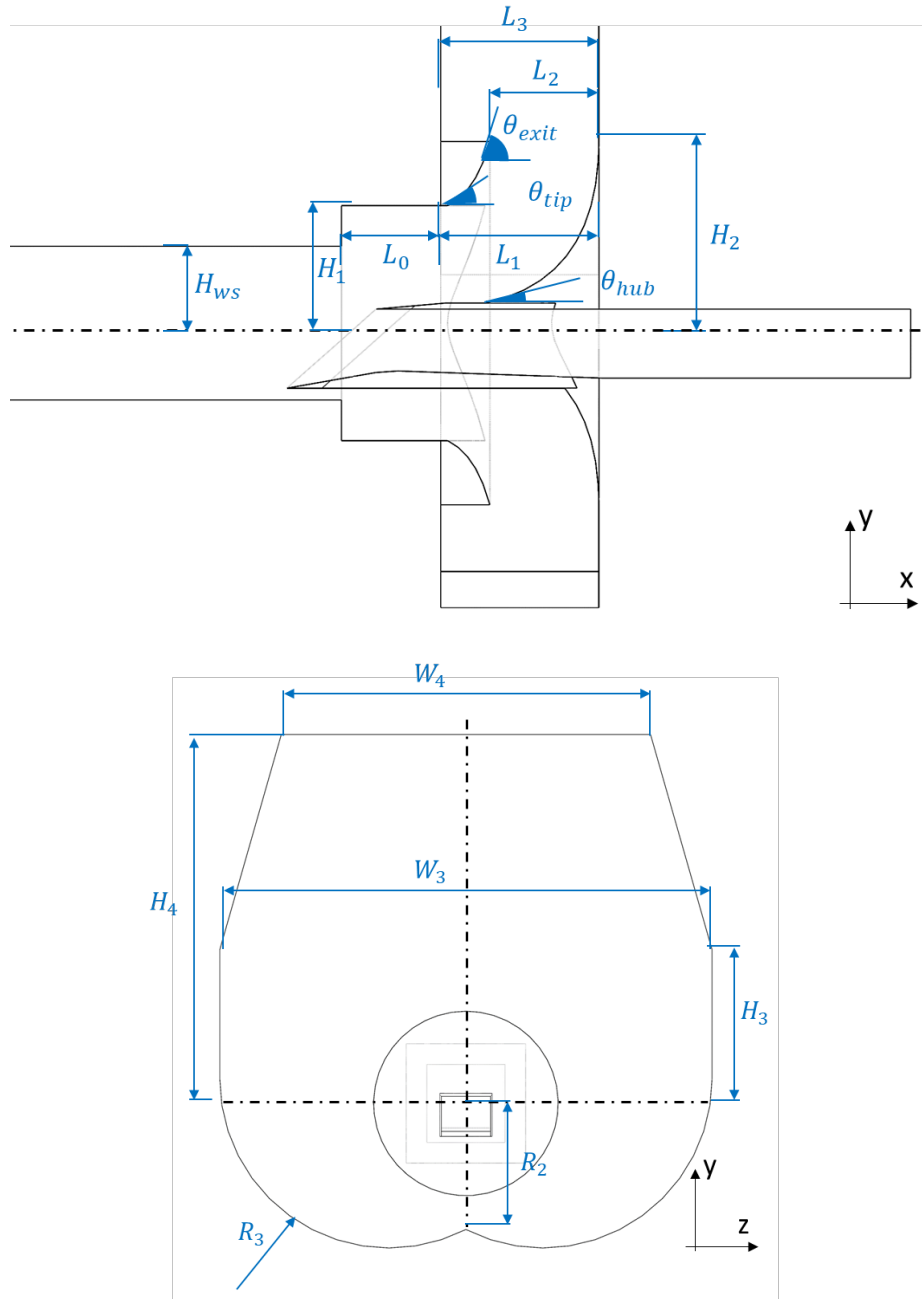
Figure 7 Working section and radial exhaust system parametric definition with a 6" equivalent AIP diameter intake installed within

A range of CFD studies aimed at a preliminary assessment of the aerodynamics of the cowl lip across the inlet operating range were conducted via 3D Euler methods using ANSYS-CFX v21.1. Euler-based simulations were chosen at this part of the work due to their shorter run times and relatively simpler grid requirements compared to RANS cases given the size of the design space needed to be explored. The installed intake performance was examined in relation to the performance of the isolated (uninstalled) configuration in terms of predicted pressure recovery at the AIP for the range of normalized mass flow ratios, ε, defined in Equation 3 (see also Figure 4):

$$\varepsilon = \frac{A_0}{A_c} = PR \cdot \left(\frac{A}{A^*}\right)_0 \cdot \left(\frac{A^*}{A}\right)_{AIP} \cdot \left(\frac{A_{AIP}}{A_c}\right) \tag{3}$$

where A^* indicates the critical area at each station which is a function of the local Mach number and PR the total pressure recovery coefficient at the AIP whose aera is indicated as A_{AIP}. The Euler based CFD provided a baseline working section geometrical configuration in terms of H_1 and L_0 parameters, with low interreference to the cowl aerodynamics for the 6" AIP intake. The baseline design parameters of the entire working section, including the exhaust system, are shown in Table 1.

Table 1 Baseline working section design parameters in relation to Figure 7 parametric definition.

L_0	$0.93 W_{in}$	θ_{exit}, deg	75º
L_1	$1.56 W_{in}$	θ_{tip}, deg	25º
L_2	$1.125 W_{in}$	θ_{hub}, deg	3º
L_3	$1.63 W_{in}$	R_2	$2.56 W_{in}$
H_1	$1.2 W_{in}$	R_3	$3.43 W_{in}$
H_2	$1.875 W_{in}$		
H_3	$3.125 W_{in}$		
H_4	$7.5 W_{in}$		

Greater emphasis was placed to the aerodynamic characteristics of the installed intake configuration at the low end of the free stream Mach number range, between M_0=1.4 and 1.8, as this is the area of operation where bypass un-starting may significantly limit the operating range (Figure 6). The representativeness of the intake aerodynamics when installed in the working section was quantified by means of the discrepancy between the installed and isolated (also referred to as "uninstalled") cowl pressure distributions. The pressure coefficient of the cowl was defined as $C_p = \frac{(p - p_\infty)}{q_\infty}$ where p was the local static pressure at the symmetry plane, outer cowl, p_∞ the free stream static pressure and q_∞ the free stream dynamic head of the supersonic flow.

The cowl Cp distributions for a normalized mass-flow of ε=0.985 (critical, or sonic, throat) and ε=0.668 (low subcritical) are shown in Figure 8 and Figure 9 respectively at a free stream Mach number of M_0=1.8 along with the corresponding flow fields for the installed and isolated cases at the symmetry plane. In the final design of the working section (Table 1), no notable variation between the AIP pressure recovery of the installed and isolated configurations is observed across the entire range of flow ratio. This indicates low interference from the walls of the working section on the steady state aerodynamics of the diffuser even at the lower end of the range for sub-critical operation. There are small differences in the spatial resolution of the cowl and terminal shocks between the two cases due to the use of a slightly coarser grid for the installed case simulations. Further Euler based CFD simulations were conducted for a free stream Mach of M_0=1.6. These results are summarised in Figure 10 for two flow ratios with ε=0.904 (Point A) and ε=0.57 (Point B). The Cp distributions near the critical operating point (Point A – bottom left in Figure 10) indicate a discrepancy between the two configurations suggesting that the bypass system influences the cowl aerodynamics with a more notable impact from 40% of the cowl length onwards. However, there is generally good agreement between the Cp distributions of the two configurations is shown at the lower part of the operating range (sub-critical operation, Point B – bottom right in Figure 10).
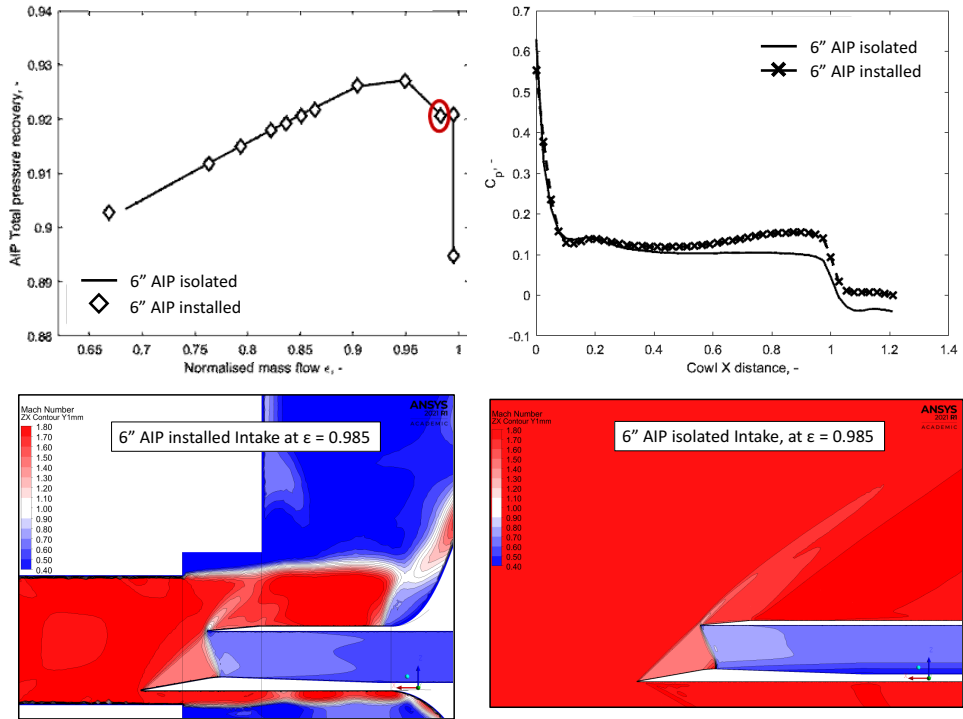
Figure 8 Cowl *Cp* distributions and corresponding symmetry plane Mach contours for the intake with ε=0.985 near the critical point in relation to the uninstalled configuration at free stream Mach number M₀=1.8
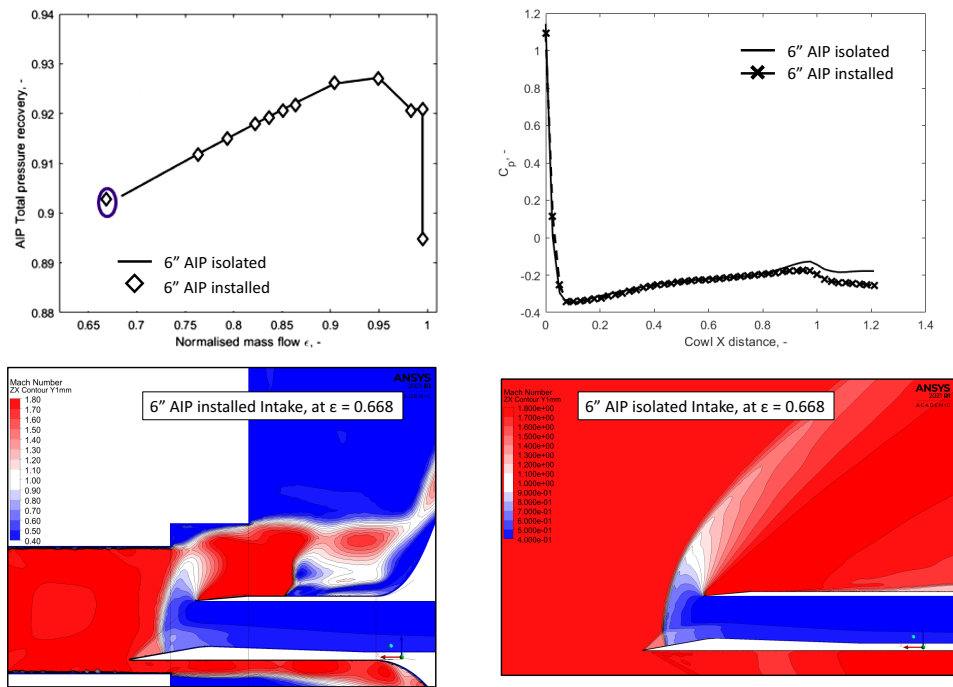

Figure 9 Cowl *Cp* distributions and corresponding symmetry plane Mach contours for the intake with ε=0.668 at sub-critical conditions in relation to the uninstalled configuration at free stream Mach number M₀=1.8
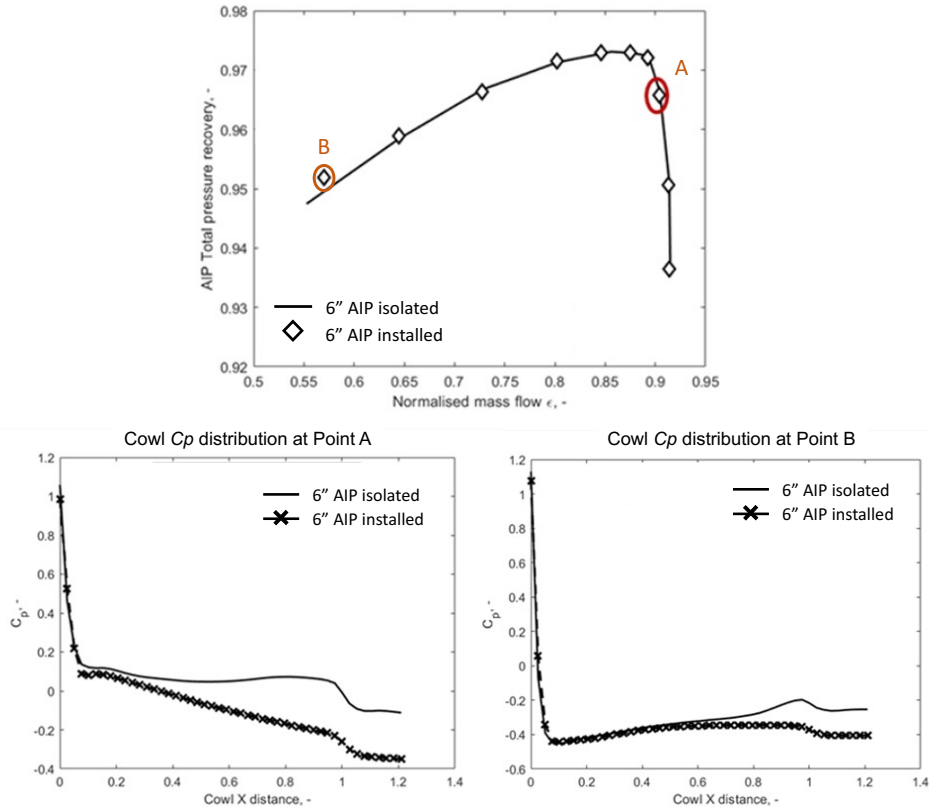
Figure 10 Intake characterstic compared to the uninstalled case across the range of flow ratios at free stream Mach number M_0=1.6 (top). Cowl Cp distribution at symmetry plane in relation to the uninstalled case at Point A, ε=0.904 (bottom-left) and Point B, ε=0.57 (bottom-right)

To further quantify the interference of the bypass section on the installed intake operation, the position of the ramp normal shock in relation to the supersonic inlet was also of interest. This, in turn can also alter the aerodynamic characteristics of the cowl lip which are directly linked to the oblique-normal shock intersection especially near the lower end of the inlet's stability limit at low flow ratios. The Euler CFD results are shown in Figure 11 for a free stream Mach number of 1.6. Continuous lines refer to the installed case while dashed lines to the isolated intake configuration. To quantify shock location, the variation of the *Cp* coefficient across the intake ramp is shown across a range of flow ratios. For M_0=1.6, differences of less than 1% are observed in the location of the oblique shock at the ramp between the installed and uninstalled configurations for all flow ratios investigated This initially suggests that there is no significant interference from the bypass system on the shape of the captured stream tube relative to the isolated case. However, Euler CFD includes no notion of the viscous boundary layers along the various walls of the test rig and as such the interactions between shock trains and boundary layers was not predicted as part of the simulation. It is expected that viscous shock boundary layer interactions would influence some of the test rig aerodynamic characteristics such as the starting range and the cowl aerodynamics, hence a RANS based CFD is necessary.

To further understand the interference of the bypass at the lower end of flow ratios for free stream Mach number of M_0=1.6 (shown in bottom left of Figure 10), further CFD investigations were carried out using RANS based models where viscous effects were accounted for. Cobalt CFD was used with the Spalart-Allmaras turbulence model with rotation/curvature corrections (SA-RC). The simulations were conducted on a structured grid with approximately 5.5 million cells. The influence of the intake's size was investigated using a baseline configuration with an equivalent AIP diameter of 6" and a scaled down configuration with an equivalent AIP diameter of 4.5".
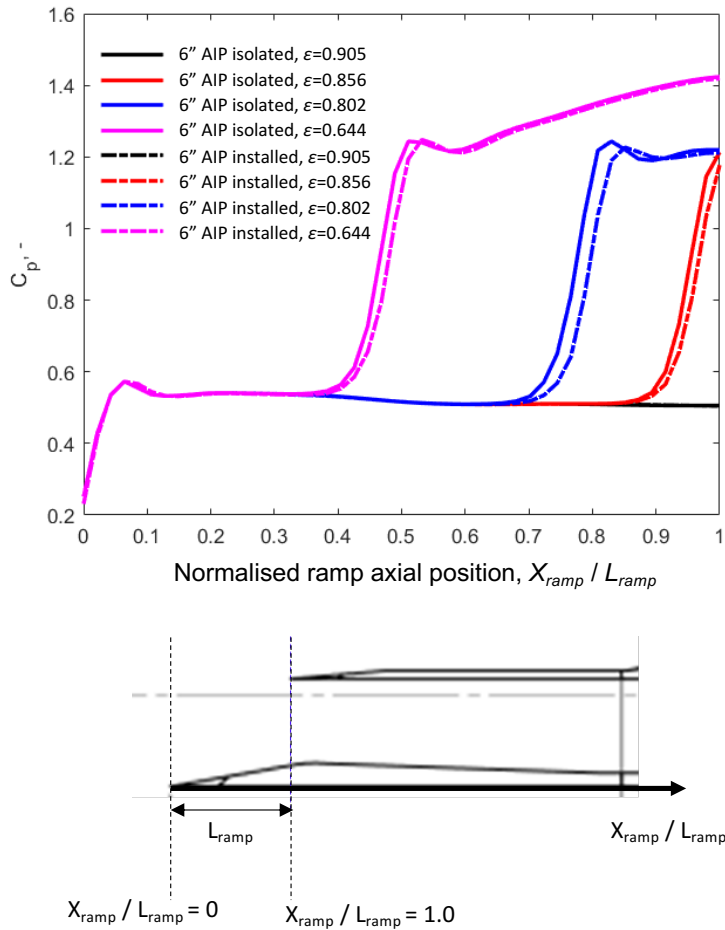
Figure 11 Cp distributions along the compression ramp indicating oblique shock location for M_0= 1.6, across the range of flow ratios for the installed and uninstalled configurations

The results from the RANS cases are summarized in Figure 12 to Figure 15 for intakes of 4.5" and 6" equivalent AIP diameter installed in the test section compared to an 'isolated' case with 6" equivalent AIP diameter. The isolated case featured a wide plate mounted below the intake at the same distance (10mm) as the wall of the test section in the installed case. This plate served both to represent the effect of the test section wall as a reflection plane and as an approach surface on which a boundary layer matching that of installed intake cases could grow.

Pressure recovery characteristics for the 6" AIP intake are shown in Figure 13. For the installed intake AIP (Figure 13) it is clear that only part of the flow ratio range can be delivered prior to a point where un-starting of the test section occurs. The lowest possible flow ratio at which the pressure recovery was representative of the uninstalled configuration (Figure 13) is approximately ε=0.7. At ε=0.67, the outermost part of the subsonic region behind the intake normal shock begins to interact with the test section wall in the vicinity of the step. This is illustrated via a Mach=1.0 iso-surface plot which shows the full extent of the sub-sonic region ahead of the intake at this condition. This shows that, for this particular intake design, lateral growth of the subsonic region will be limiting for wall interaction. This interaction increases further in extent as mass flow is reduced and at ε=0.56 the whole shock system lies ahead of the intake, at which point the test section is, un-started. Further longitudinal adjustment of the position of the test section step may improve the operating range slightly. However, interaction with the wall would be replaced by interaction with the step expansion which could also be significant.
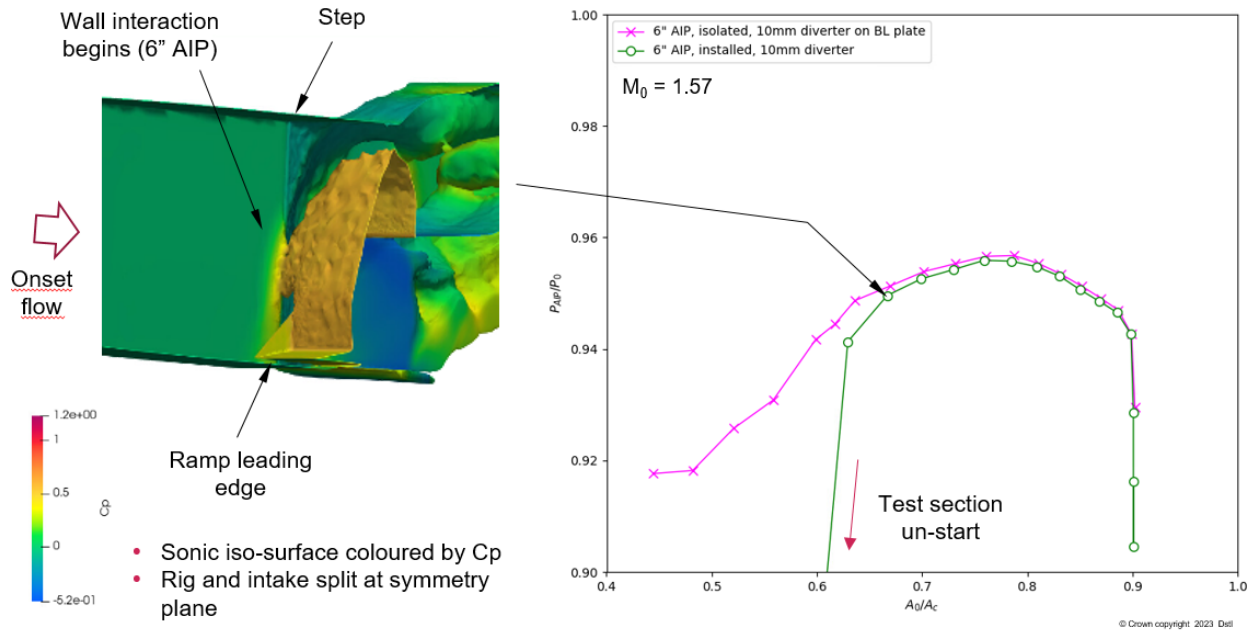
13

Figure 12 Comparison of intake pressure recovery characteristics for the 6" AIP isolated and installed cases

The characteristic of the 4.5" equivalent AIP diameter intake is added to the same chart with a red curve in Figure 13. The is almost fully aligned with the uninstalled, 6" AIP case with the boundary layer plate in place, suggesting that the wall interaction would cause no significant issues in terms of either un-starting or representativeness of the 4.5" configuration. These simulations indicate that no wall interference occurs above a flow ratio of $\varepsilon=0.52$, which would represent the entire useful working range of an external compression intake of this type (lower limit of $\varepsilon=0.55$ for a typical gas turbine engine installation).
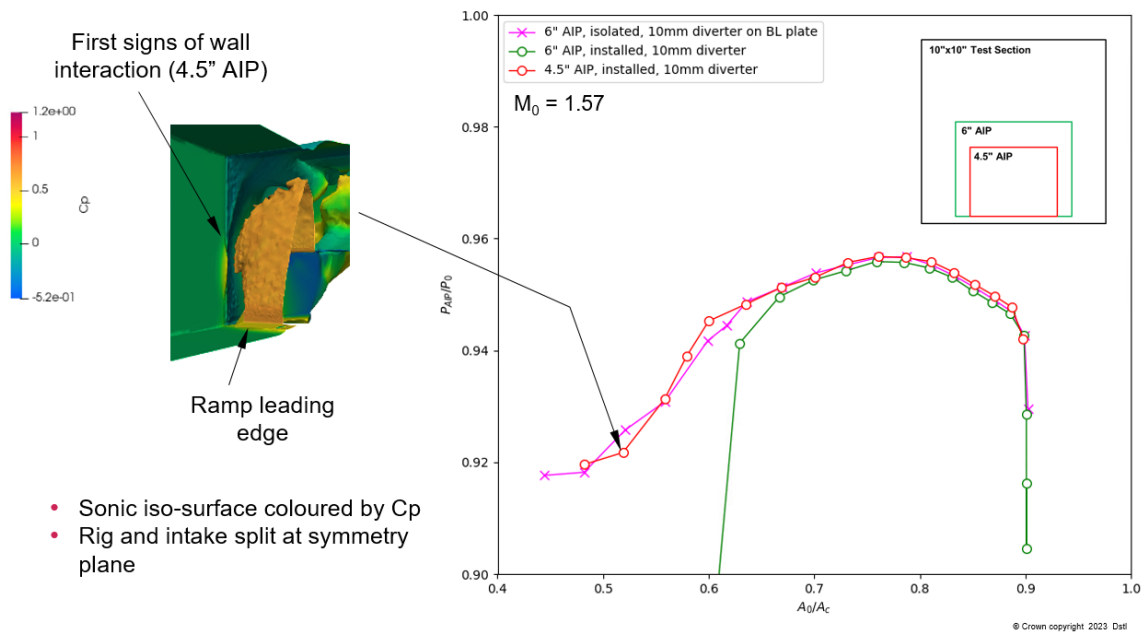

Figure 13 Comparison of intake pressure recovery characteristics of the 4.5" and 6" AIP installed cases with the 6" isolated case

The Mach=1.0 iso-surface plot in Figure 13 shows that, even at this reduced intake size, lateral growth of the intake subsonic region is still the limiting case for wall interaction with the first signs of interaction being seen at around ε=0.52. Further investigation of the break in the trend of the pressure recovery characteristic at about ε=0.6 (red and pink curves, Figure 14) reveals that this is due to the onset of flow separation in the corner region downstream of the intake throat. The reason for this separation is likely to be ingestion of a small amount of the onset boundary layer. The diverter height was set at a nominal 10 mm, but the boundary layer thickness was 14.2mm at the tip of the intake ramp. This separation was absent in a similar calculation for the isolated 6" AIP intake without the boundary layer plate. Whilst this would be an undesirable feature in a real intake design, it is reassuring that this same feature was captured in both the isolated (6" AIP) and installed (4.5" AIP) cases where mass flow ratios in this range were possible.
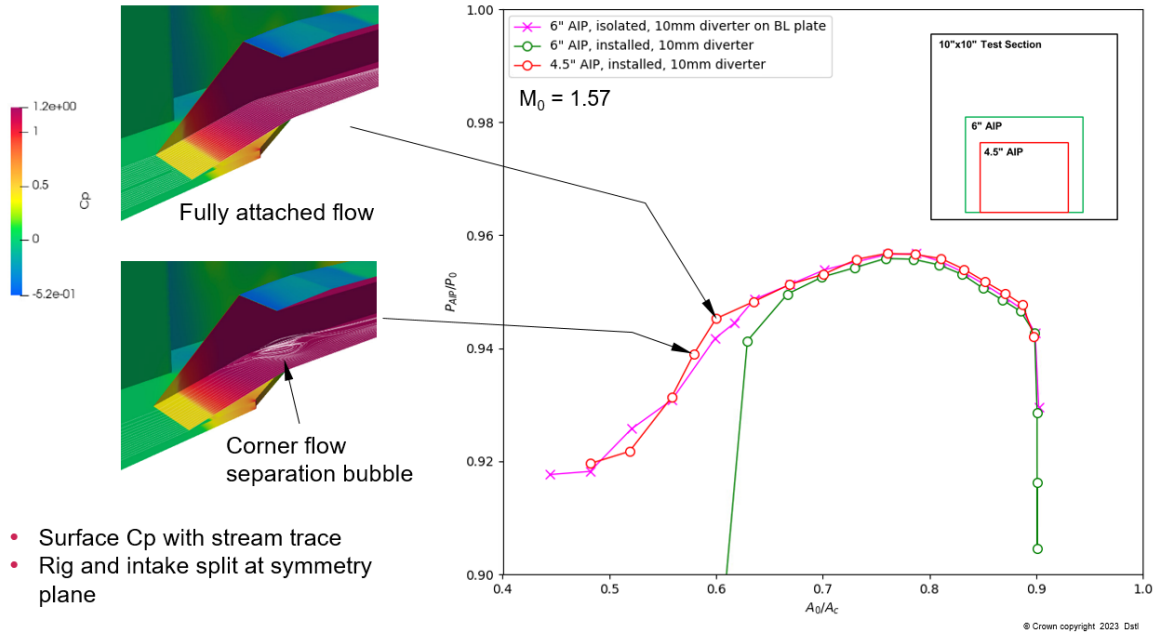

Figure 14 Onset of a corner flow separation bubble downstream of the intake throat

The viscous CFD results for both intake sizes are summarised in Figure 15, along with the ranges across which optical measurements at the AIP are likely to be feasible. The results indicate that the selected working section size and configuration will enable testing of a 4.5" equivalent AIP diameter intake duct across its entire range of operation without significant penalties on the representativeness of the aerodynamics around the supersonic entry. A slightly larger AIP diameter intake, where optical measurements would be less challenging, would deliver approximately 50% of its operating range when installed in the test section without notable penalties in its aerodynamic characteristics.
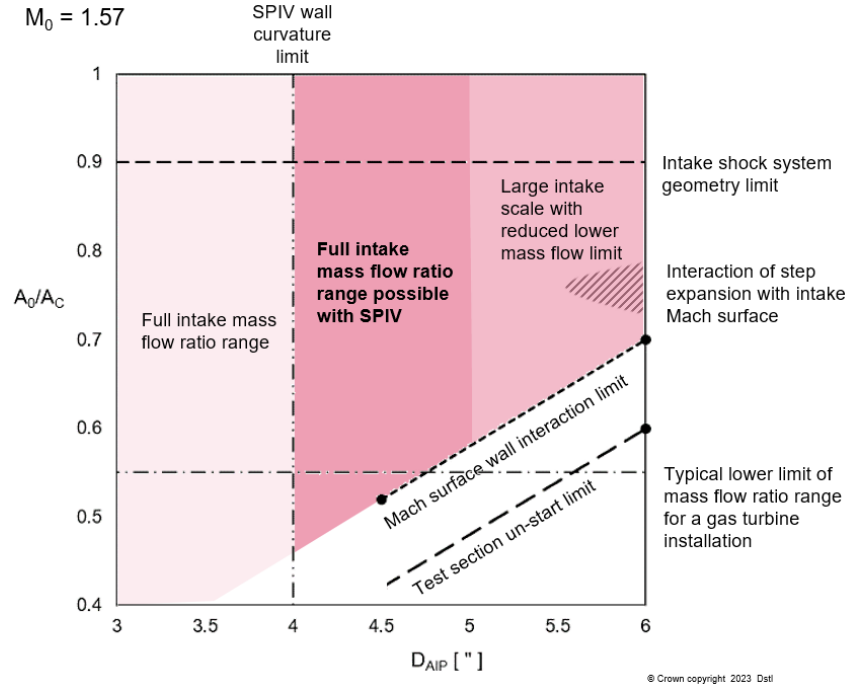
Figure 15 Summary of estimated intake operating range at M_0=1.57 for the range of AIP diameters indicating areas where optical measurements are feasible

In order to understand the influence of the radial bypass collector system on the intake aerodynamics and to specify a preliminary design for this section, RANS simulations were used to explore the design space at the lower end of the required operating range with free stream Mach number of M_0=1.6. The nozzle system including the settling chamber and pre-contraction components were included in these CFD models to capture the development of the incoming boundary layers along the inflow part of test rig. Modelling the incoming boundary layer at the lower range of free stream Mach numbers is key to understand potential un-starting issues of the system hence it was important for this to be included as part of the CFD simulations. The computational domain and a detail of the working section meshed are shown in Figure 16 for a 6" AIP intake. The unstructured computational grid was generated in Cadence Pointwise v18.5 using the T-rex functionality which produced a total grid size of ~112 million nodes with $y^+<1$ across all viscous walls of the entire domain. The grid generation process was scripted to enable grid adaptation to the design variations investigated. The simulations used the k-ω turbulence model with adiabatic walls and second order advection and turbulence numerical schemes. Total pressure inlet was used as a boundary condition at the subsonic settling chamber inlet, with static pressures at the two outlets of the domain namely the exit of the bypass system and the exit of the intake's subsonic diffuser. These simulations provided the characteristics of the free stream boundary layer at the working section by the nozzles and were used to adjust the diverter height to ensure that no part of the incoming boundary layer enters the duct. The thickness of the boundary layer at the symmetric plane of the domain upstream of the intake is qualitatively shown in Figure 17 in terms of density gradient along the y-axis. The normalised boundary layer thickness between the nozzle exit, defined as the axial position where the walls become parallel, and the ramp is shown in Figure 18, which yields a boundary layer thickness of approximately 14.2 mm at the base of the intake ramp and a boundary layer growth rate of approximately 1.7 mm/m. This result shows that the 10 mm diverter height used for these cases was not sufficient to prevent a small amount of boundary layer ingestion by the intake. This resulted in instabilities of the shock system upstream of the throat and partially destabilised the operation of the intake.
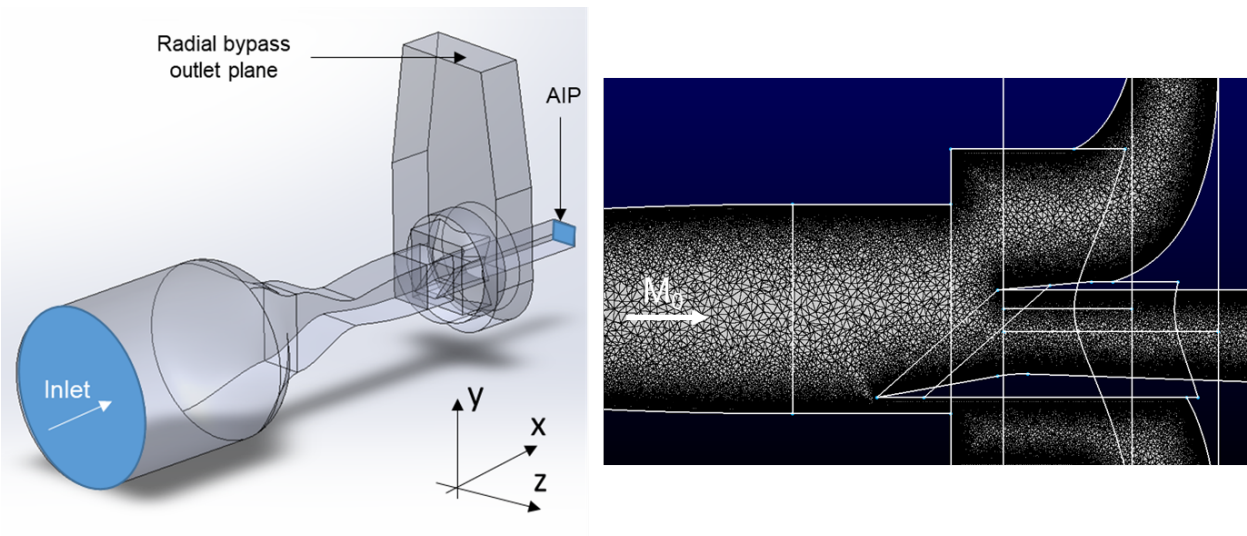
16

Figure 16 Computational domain comprising full nozzle system, working section and exhaust (left). Detail of viscous unstructured grid in the working section with the aircraft intake installed within (right)
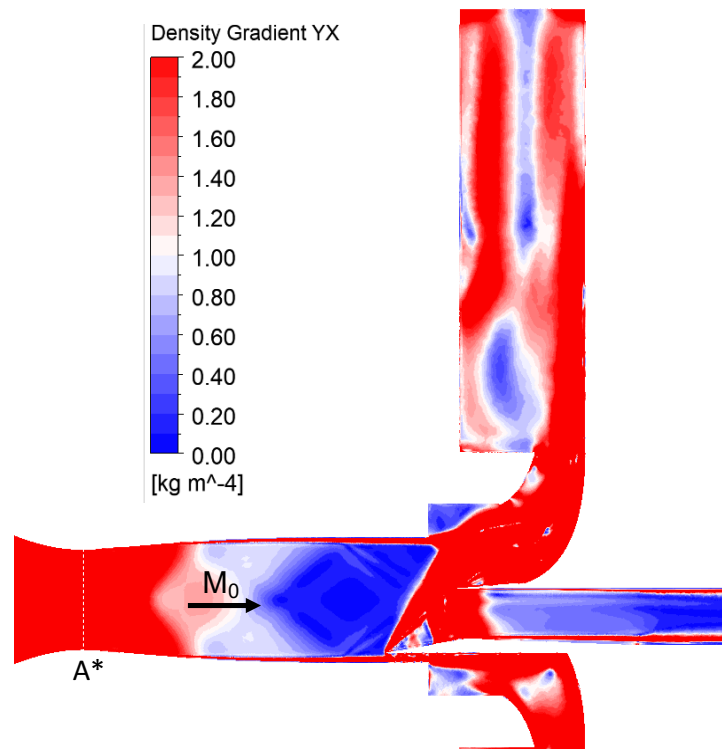

Figure 17 Density gradient distribution across the supersonic section of the test rig for free stream Mach M_0=1.6 and intake flow ratio ε=0.843
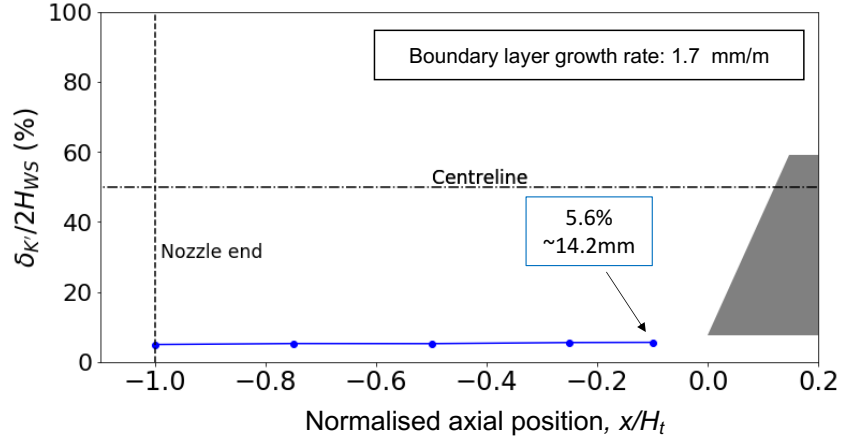
Figure 18 Non-dimensional boundary layer thickness, δκ/2Hws, variation at the lower wall between nozzle exit and intake installed in the working section for free stream Mach M0=1.6. Ht is intake throat height, Hws is the working section height.

A critical geometric characteristic of the radial collector system directly linked with its overall size and volume is the overall width, W_3, of the collector (Figure 7). An initial, coarse exploration of the design space was conducted to quantify the influence of the width on the total pressure loss, expressed as the residence time of the flow inside this domain. Previous work has indicated that long residence times in radial exhaust systems for steam turbines correlate with pressure loss as it is linked to large, localised recirculating flow regions in various key positions of the domain [21][22]. The residence time is affected by the W_3 (Figure 19), where a range of W_3 between $10W_{in}$ and $5W_{in}$ was explored (where W_{in} is the intake width of 160mm, Figure 4) for free stream Mach number M_0=1.6 at intake flow ratio ε=0.843. These simulations indict that the notable mitigation of flow recirculation inside the exhaust section for a domain with W_3=$5W_{in}$, reduces the total pressure loss coefficient of this section by approximately 20% compared to the baseline configuration with W_3=$10W_{in}$. Based on the parametric definition shown in Figure 7, the design parameters of the exhaust system that was kept constant across the cases shown in Figure 19 is summarised in Table 2.
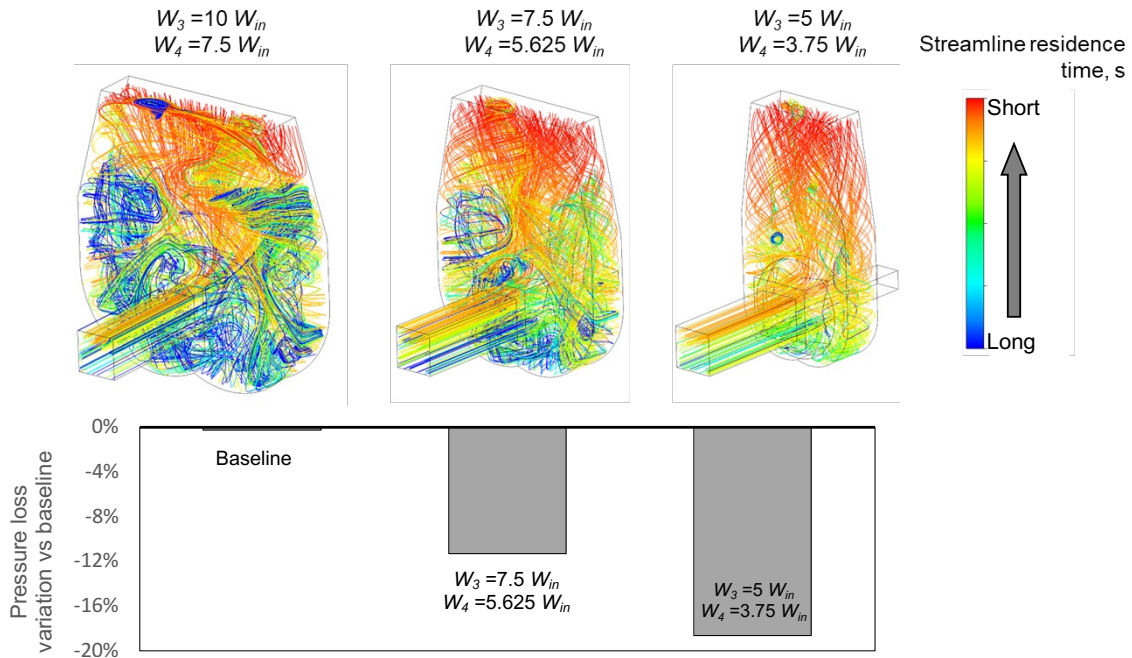

Figure 19 Influence of exhaust section's width W_3 on flow residence time prior to be exhausted from the domain for free stream Mach M_0=1.6 and flow ratio ε=0.843

18

Table 2 Working section design parameters in relation to Figure 7 parametric definition used to determine W_3 and W_4 for minimum pressure loss.

L_0	$0.93 W_{in}$	θ_{exit}, deg	75°
L_1	$1.09\ W_{in}$	θ_{tip}, deg	25°
L_2	$0.65\ W_{in}$	θ_{hub}, deg	3°
L_3	$1.63\ W_{in}$	R_2	$1.93\ W_{in}$
H_1	$1.2\ W_{in}$	R_3	$1.875\ W_{in}$
H_2	$1.875\ W_{in}$		
H_3	$3.125\ W_{in}$		
H_4	$7.5\ W_{in}$		

Finally, the importance of flow quality at the onset of the supersonic entry, yields the requirement to quantify the flow characteristics at this position. One pertinent way to do so at a preliminary level of analysis prior to more sophisticated assessments, is via the flow angularity as discussed in [23] and also shown in [24] and [25]. This flow angularity (or swirl angle) in this case is defined as the angular deviation of the azimuthal flow velocity, u_θ, from the axial direction at a fixed radial position, $\tan^{-1}(u_\theta/u_x)$. The nozzle exit plane is indicated in Figure 20 as Plane A, located one intake throat height (H_t) upstream of the leading edge of the intake ramp and is defined as the axial position downstream of the nozzle throat where the walls become parallel. The cross-flow swirl angle distributions between Plane A and Plane H ($0.25H_t$ upstream of ramp) indicate a maximum deviation from the axial direction of about +/- 0.2 deg suggesting that the designed supersonic nozzle generates acceptable flow quality at the onset planes. However, more analysis is required to fully characterize the incoming flow that would include the evaluation of the pressure loss distribution across the plane and the influence of the growing boundary layers on the centerline Mach number variation.
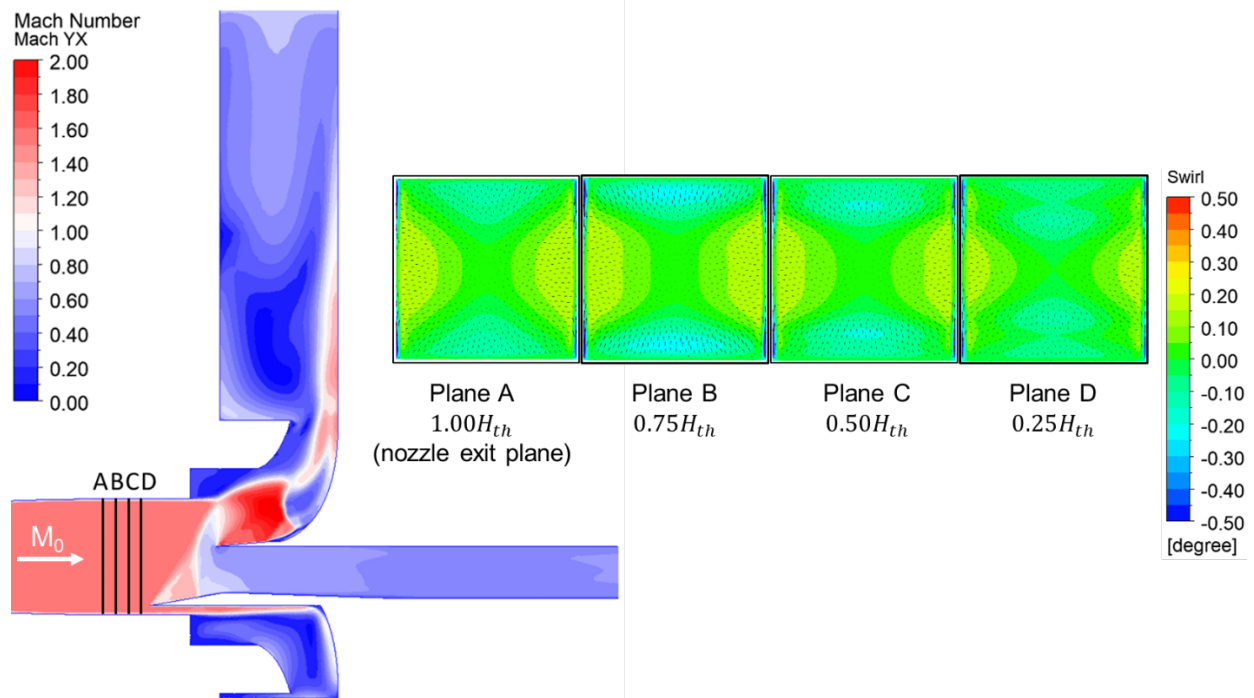

Figure 20 Cross-flow swirl angle distributions at four axial positions between nozzle exit and intake ramp

V. Conclusions and future developments

The conceptual and preliminary design and sizing of an intermittent, blowdown supersonic test rig aimed at intake distortion simulation between free stream Mach numbers 1.4 – 3.0 was presented. An overview of the plant design to generate the high-pressure flow was provided along with the estimated productivity in terms of run and recharging time. The influence of the working section on the aerodynamics and operating range of an external compression, rectangular supersonic intake was assessed. This is a key aspect of the design activity, as the details of the aerodynamics of the intake can adversely affect the representativeness of the unsteady distortion characteristics. This is of particular concern near the stability limit of the test model. CFD simulations were carried out primarily focused on the low end of free stream Mach number operation between 1.6 and 1.8. The simulations indicated that a working with a semi-confined jet upstream of the intake model enables fully representative testing of test models up to about 4.5" equivalent AIP diameter without significant interference of the walls on the aerodynamic characteristics of the model across the entire operating range. Half of the required operating range could be achieved for larger test models of up to 6" equivalent AIP diameter. A design concept and a first, coarse design space exploration for the bypass system indicates that a 'wrap-around' exhaust hood can divert the spilled flow radially without a large penalty in terms of pressure loss. Further optimization of this system will enable a large part of the subsonic diffuser to be accessible for the installation of instrumentation, but more importantly it will enable unobstructed line of sight to the AIP for optical measurements. The next step is to expand the CFD studies to cover the entire desired range of operation up to Mach 3.0 and the detailed design of the system including the noise attenuation system.

Acknowledgements

References

[1] Society of Automotive Engineers. *Inlet Total-Pressure-Distortion Considerations for Gas-Turbine Engines.* SAE Aerospace Information Report 1419c, 2017. https://doi.org/10.4271/air1419c.

[2] Society of Automotive Engineers. *A Methodology for Assessing Inlet Swirl Distortion.* SAE Aerospace Information Report 5686, 2007. https://doi.org/10.4271/air5686.

[3] Williams, M., and Stevens, K. "Computational Prediction of Subsonic Intake Spillage Drag." *24th AIAA Applied Aerodynamics Conference*, 2006. https://doi.org/10.2514/6.2006-3871.

[4] Kimzey, W. F., and Ellis, S. H. "Supersonic Inlet Simulator - A Tool for Simulation of Realistic Engine Entry Flow Conditions." 1974. https://doi.org/10.4271/740824.

[5] Surber, L., Syberg, J., Koncsek, J., "Performance of Highly Integrated Inlets for Supersonic Aircraft," *AGARD Conference Proceedings No. 301*, May 1981.

[6] Fisher, S. A., and Ford, D. J. *An Investigation of Starting Problems in a Specialised Wind Tunnel for Testing a Rectangular Mixed Compression Intake at Mach 3.* Publication 138. Aeronautical Research Laboratories Mechanical Engineering, Department of Supply, Australian Defence Scientific Service, 1972.

[7] McLelland, G., MacManus, D. G., Zachos, P. K., Gil-Prieto, D., and Migliorini, M. "Influence of Upstream Total Pressure Profiles on S-Duct Intake Flow Distortion." Journal of Propulsion and Power, Vol. 36, No. 3, 2020. https://doi.org/10.2514/1.b37554.

[8] Migliorini, M., Zachos, P. K., and MacManus, D. G. "Novel Method for Evaluating Intake Unsteady Flow Distortion." Journal of Propulsion and Power, 2021, pp. 1–13. https://doi.org/10.2514/1.b38127.

[9] Doll, U., Migliorini, M., Baikie, J., Zachos, P. K., Röhle, I., Melnikov, S., Steinbock, J., Dues, M., Kapulla, R., MacManus, D. G., and Lawson, N. J. "Non-Intrusive Flow Diagnostics for Unsteady Inlet Flow Distortion Measurements in Novel Aircraft Architectures." Progress in Aerospace Sciences, Vol. 130, 2022, p. 100810. https://doi.org/10.1016/j.paerosci.2022.100810.

[10] Gnani, F., *Investigation on Supersonic High-speed Internal Flows and the Tools to Study their Interactions*. University of Glasgow, PhD thesis, 2018.

[11] Sabnis, K., Babinsky, H., Galbraith, D. S., and Benek, J. A. "Nozzle Geometry-Induced Vortices in Supersonic Wind Tunnels." *AIAA Journal*, Vol. 59, No. 3, 2020, pp. 1–12. https://doi.org/10.2514/1.j059708.

[12] Pope, A., Goin, KL., *High Speed Wind Tunnel Testing,* John Wiley & Sons, London, 1965.

[13] Roach, P. E. "The Generation of Nearly Isotropic Turbulence by Means of Grids." International Journal of Heat and Fluid Flow, Vol. 8, No. 2, 1987, pp. 82–92. https://doi.org/10.1016/0142-727x(87)90001-4.

[14] Grenson, P., and Beneddine, S. "Analysis of Shock Oscillations of an External Compression Supersonic Inlet through Unsteady Numerical Simulations," AIAA 2018-3011, *2018 Applied Aerodynamics Conference*, June 2018. https://doi.org/10.2514/6.2018-3011.

[15] Trapier, S., Deck, S., Duveau, P., and Sagaut, P. "Time-Frequency Analysis and Detection of Supersonic Inlet Buzz," AIAA Journal, Vol. 45, No. 9, 2007, pp. 2273–2284. https://doi.org/10.2514/1.29196.

[16] Trapier, S., Duveau, P., and Deck, S. "Experimental Study of Supersonic Inlet Buzz," AIAA Journal, Vol. 44, No. 10, 2012, pp. 2354–2365. https://doi.org/10.2514/1.20451.

[17] Sasson, J., "Small Scale Mass Flow Plug Nozzle Calibration," NASA/CR – 2015-218820, July 2015. https://ntrs.nasa.gov/api/citations/20150014965/downloads/20150014965.pdf

[18] Davis, D.O., Friedlander, D.J., Saunders, J.D., Frate, F.C., & Foster, L.E., "Calibration of the NASA GRC 16″ Mass-Flow Plug," Proceedings of the ASME 2012 Fluids Engineering Division Summer Meeting collocated with the ASME 2012 Heat Transfer Summer Conference and the ASME 2012 10th International Conference on Nanochannels, Microchannels, and Mini channels. Volume 2: Fora. Rio Grande, Puerto Rico, USA. July 8–12, 2012. pp. 269-277. https://doi.org/10.1115/fedsm2012-72266.

[19] Seddon, J., and Goldsmith, E. "Intake Aerodynamics, Second Edition." 1999. https://doi.org/10.2514/4.473616.

[20] Davis, T. W. "Review of Transonic Wall Interference Corrections and Considerations for Development." *AIAA Aviation 2019 Forum*, 2019. https://doi.org/10.2514/6.2019-3094.

[21] Burton, Z., Ingram, G. L., and Hogg, S. "A Literature Review of Low-Pressure Steam Turbine Exhaust Hood and Diffuser Studies." *Journal of Engineering for Gas Turbines and Power*, Vol. 135, No. 6, 2013, p. 062001. https://doi.org/10.1115/1.4023611.

[22] Wang, H., Zhu, X., Du, Z., and Yang, H. "Aerodynamic Optimization System Development for Low Pressure Exhaust Hood of Steam Turbine." *Volume 7: Turbomachinery, Parts A, B, and C*, 2010, pp. 2139–2148. https://doi.org/10.1115/gt2010-22280.

[23] Titchener, N. "An Experimental Investigation of Flow Control for Supersonic Inlets," *PhD thesis*, Cambridge University, 2013.

[24] Loth, E., Titchener, N., Babinsky, H., and Povinelli, L. "Canonical Normal Shock Wave/Boundary-Layer Interaction Flows Relevant to External Compression Inlets." *AIAA Journal*, Vol. 51, No. 9, 2013, pp. 2208–2217. https://doi.org/10.2514/1.j052175.

[25] Sabnis, K., Galbraith, D., Babinsky, H., and Benek. JA., "Flow Characterisation for a Validation Study in High-speed Aerodynamics," AIAA 2019-3073. *AIAA Aviation 2019 Forum*, June 2019.